agriculture

MDPI

Article

Geometric Analysis of Greenhouse Roofs for Energy Efficiency Optimization and Condensation Drip Reduction

Araceli Peña-Fernández [1,*], Manuel A. Colón-Reynoso [1] and Pilar Mazuela [2]

[1] CIAIMBITAL Research Centre, Engineering Department, University of Almería, Carretera de Sacramento s/n, 04120 Almería, Spain; mcr535@inlumine.ual.es
[2] Departamento de Producción Agrícola, Facultad de Ciencias Agronómicas, University of Tarapaca, Arica 1010072, Chile; pmazuela@academicos.uta.cl
* Correspondence: apfernan@ual.es

Abstract: Greenhouses are instrumental in the advancement of regions globally. The geometric arrangement of these structures plays a pivotal role in governing sunlight distribution, facilitating ventilation, and managing condensation. The roof's shape significantly affects energy efficiency and the accumulation of condensation water, which, when dripping onto crops, can induce diseases and diminish production. This study introduces a Matlab program designed for defining and analyzing greenhouse roof geometry that is adaptable to both single-span and multispan structures. Various roof shapes were examined, and angles along their length were determined to facilitate condensation droplet runoff. In the ogival roof shape, water droplets adhering to the roof surface were found to slide off, preventing interior dripping. However, in all semicylindrical roof structures, dripping occurred on more than 50% of the cultivated ground surface. Furthermore, the greenhouse's energy efficiency was evaluated by analyzing diverse roof models, accounting for the surface area and internal air volume. There was little difference in the volume of air inside the greenhouse attributable to the roof shape. Increasing the arch height relative to the span width enhanced solar energy capture and the roof surface, with the semicylindrical shape being more efficient in this case. The results aim to aid in the selection of the optimal greenhouse type based on the climate and latitude. This study offers a valuable decision-making tool for the planning and design of agricultural structures, providing insights to enhance their overall sustainability and performance in diverse environmental contexts. Hence, in cold climates and high latitudes, the steeper roof angle of the ogival shape type 2*l* and its smaller surface area promote solar energy capture and reduce convective heat losses. In warmer climates, a larger roof surface facilitates natural cooling, making the ogival shape type 3*l*/2 recommended.

Keywords: greenhouse; energy efficiency; roof; condensation

Citation: Peña-Fernández, A.; Colón-Reynoso, M.A.; Mazuela, P. Geometric Analysis of Greenhouse Roofs for Energy Efficiency Optimization and Condensation Drip Reduction. *Agriculture* **2024**, *14*, 216. https://doi.org/10.3390/agriculture14020216

Received: 31 December 2023
Revised: 24 January 2024
Accepted: 27 January 2024
Published: 29 January 2024

1. Introduction

Greenhouse cultivation is widespread globally, driving the economies of many regions. Presently, China boasts the largest greenhouse cultivation area, with the highest concentration found in southeastern Spain [1]. The expansion of greenhouse cultivation responds to the need to feed a growing population under economic, environmental, and social criteria.

To achieve sustainable development in intensive greenhouse agriculture, it is crucial to design structures based on the climate of the installation area [2]. This involves maximizing the utilization of solar energy and reducing energy consumption. An appropriate plastic covering can reduce the annual energy demand by up to 9.8% in cooling and 6.3% in heating [3]. Other influencing factors to achieve this objective include greenhouse orientation, angle, and roof geometry.

The orientation of the greenhouse's longitudinal axis influences the amount of intercepted solar radiation. Various studies have shown that a North–South orientation captures

more solar radiation throughout the year compared to an East–West one, a trend generally observed at all northern latitudes, leading to significant differences in energy savings ranging from 2% to 28% as the latitude increases [4–8]. During summer in temperate climates and middle latitudes, the interior temperature of an East–West-oriented greenhouse is 3 to 5 °C lower than that of a North–South orientation. Additionally, during winter, the total solar radiation gain is greater throughout the day in an East–West orientation, resulting in reduced energy consumption for heating in winter and cooling in summer [9–11], with significant savings in cooling expenses of up to 9.28% [12].

Research results demonstrate that the temperature inside the greenhouse is dependent on the shape of the greenhouse cover [6]. The angle and geometry of the cover influence the capture of solar energy and the energy consumption of the greenhouse to a greater or lesser extent depending on the latitude and climatic conditions [13]. Higher cover angles enable increased solar radiation input during winter, when the sun is low, and decrease it in summer, when the sun is high. In cold climates and northern latitudes, the total solar gain inside the greenhouse increases with the angle of inclination and the surface area of the cover.

The different geometric cover shapes based on the annual amount of captured solar radiation include, in decreasing order, elliptical, asymmetrical, gable, semicircular, and Gothic forms [14]. Greenhouses with an asymmetrical cover receive annually between 8.4 and 11.3% more solar radiation than gable greenhouses, while arched and quonset forms receive 1.8% and 11.6% less, respectively [6,7]. Gothic and ogival-shaped covers are the most efficient at capturing solar energy for cold climates and high latitudes [14]. In warm climates and middle latitudes, arched covers receive the least annual radiation and would be more appropriate when energy needs are higher due to cooling [12,15,16].

The efficiency of capturing solar radiation varies among different greenhouse cover shapes depending on the season. During winter, greenhouses with arched and asymmetrical covers capture 6.2% and 5.7% more solar radiation, respectively, than gabled greenhouses. In contrast, during summer, arched covers receive 1.8% less solar radiation, while asymmetrical covers receive 9.7% more solar radiation than gabled greenhouses [17]. Therefore, considering this seasonal behavior, in arid climates, a greenhouse should be designed to receive minimal radiation in summer and maximum radiation in winter [16].

On the other hand, the angle of the greenhouse cover, regardless of its geometric shape, plays a crucial role in its energy efficiency. Recommended angles depend on the latitude and climate of the location. Generally, the optimal angle to increase the amount of captured solar radiation is between 18° and 30° [14,18]. Scale experiments in multispan greenhouses with a gabled cover have found that the optimal cover angle is 30° [19]. However, in arid areas like Qatar, a cover inclination of 26.5° is recommended [16]. In mid-to-high latitudes, a value of 45° is suggested, measured at the base of the cover [20], although it should be considered over its entire curved surface [21]. Other studies have shown that the overall light transmittance of the greenhouse increases with the angle of the cover up to values of 28° to 32°, beyond which it barely changes, and the accumulation of energy due to solar radiation on the greenhouse floor decreases [22]. The cover angle is implicitly considered through the ratio Z, defined as the height of the greenhouse/span width, with studies finding that solar radiation interception increases with increasing Z [15], compensating for part of the decrease that occurs with increasing latitude.

The energy efficiency of the greenhouse relies on the balance between capturing solar energy and the heat losses that occur through the cover and walls, especially when these need to be offset through heating and cooling systems. About 40% of heat losses primarily occur through conduction and convection across the greenhouse's outer surface [5,7]. In cold climates, the larger the cover surface, the more the energy needed to heat the greenhouse interior [17]. The heating energy consumption of a gabled greenhouse is 8% lower than that of a semicylindrical one [11] and between 2.6% and 4.2% higher than that of a Gothic-shaped greenhouse [4]. In temperate climates, the Gothic-shaped cover is more energy-efficient compared to gabled and semicylindrical covers [23].

Natural ventilation is the primary cooling system used by most greenhouses in warm climates, with better results achieved by semicircular-shaped greenhouses compared to gabled ones [12]. Increasing the ventilation ratio results in a higher temperature and relative humidity inside the semicircular cover compared to the Gothic shape, with the situation reversing during summer [24].

The ratio between the exterior surface of greenhouses and the cultivated soil surface is lower in multispan greenhouses than in single-span ones, reducing heat losses through the walls and heating energy consumption by 4–10% [25]. The opposite occurs in warm climates, where cooling needs prevail over heating [12].

The number of spans and the width of spans influence solar energy gain and energy consumption in the greenhouse. Increasing the span width reduces the amount of solar radiation captured by a single-span greenhouse by up to 35% in winter and 23.4% in summer [7]. In multispan greenhouses, decreasing the span width only results in an 8% and 3% reduction in solar radiation entering the greenhouse in winter and summer, respectively. However, the decrease in energy consumption with increasing span width is significant in cold climates, decreasing by 13.4% and 3.5% in single-span and multispan greenhouses, respectively [17].

The ratio (width/length) of the greenhouse influences its energy efficiency when using the cooling system with evaporative panels. It has been found that when the ratio is 1:3, the interior temperature along the longitudinal axis of the greenhouse is lower than when the ratio is 3:4 [16].

The angle of the greenhouse cover influences its luminous and thermal performance, especially during winter when the sun is low [26]. It also plays a role in reducing condensation on the cover, which can cause damage to crops and decrease light transmission through plastic materials [27,28]. At the same time, condensation increases diffuse radiation inside the greenhouse [29], which can favor certain crops and decrease the yield of others, such as microalgae [30].

The use of plastics containing antifog/antidrip additives as greenhouse cover material improves light transmission but comes with the drawbacks of high cost and low durability [31]. Reducing condensation results in a higher plant growth rate and more abundant crops, which can be achieved with a cover angle that encourages the sliding of condensed water.

A water droplet begins to slide on a surface when the contact angle exceeds its most stable value (Figure 1), which is constant and determines the shape of the droplet [32–34].

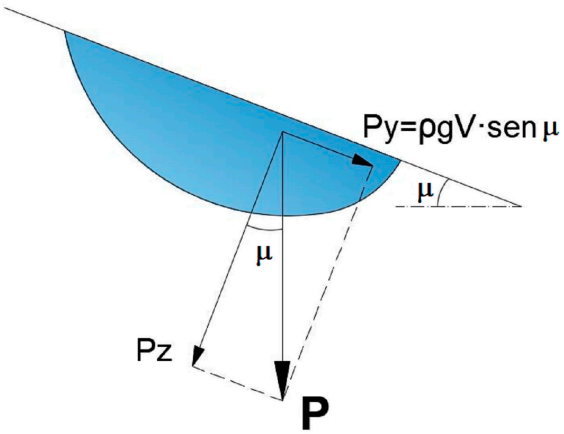

Figure 1. Forces on a hanging droplet.

The minimum incline value of a surface, denoted as μ, on which a water droplet adheres and from which it begins to slide, has been determined by various authors through simulation techniques as $\mu \geq 30^{\circ}$ [35] or through laboratory experiments as $\mu > 28^{\circ}$ [36]. Ad-

ditionally, a surface with a 30° inclination not only promotes droplet sliding but also facilitates water collection by gravity [37,38], which is particularly relevant in water-scarce areas.

It has been deduced that the inclination required for a water droplet to slide on a polyethylene surface is lower when its volume is larger [39]. Increasing the inclination reduces the required droplet size to initiate movement [40], and the maximum radius the droplet reaches when it starts to fall is inversely proportional to the roof's incline angle [41]. The minimum water volume value for a sliding droplet is obtained for a vertical surface $\mu_c = 90°$ [42].

The objective of this study was to investigate various design parameters influencing the energy efficiency of greenhouses and reduce the amount of water condensing on the roof. We considered only roof shapes suitable for multispan greenhouses. We developed a Matlab (Software version: R2020b Update 7) program that allowed us to calculate, for any span width and arch height, the angle and surface for gothic, semicylindrical, and gable roof types, among others. Additionally, we calculated the cultivation surface where dripping occurs, the air volume, and the optimal greenhouse length.

2. Materials and Methods

2.1. Greenhouse Roof Geometry

Equations defining the geometry of greenhouse roofs are valuable for structural calculations and the energy balance of the greenhouse. With the designed Matlab program, we can calculate the length of each arc segment and the angle at each point for any roof geometry formed by one or two arcs. The parameters defining the geometry of a greenhouse bay are as follows: width, l; ridge height, t; arch height, f; and pillar height, h. The arch height, f, is defined as $f = t - h$.

2.2. Geometric Analysis of Semicircular Arch Structures

The geometric analysis of arches allows the optimal solution to be found that maintains the aesthetic and resistant characteristics [43] as well as other functional characteristics, such as those addressed in this paper.

The roof of a semicircular greenhouse can vary from a semicircle, f = r, where r is the radius of the circle, to a flat roof when f = 0, passing through a lowered arch [44] with $0 < f < r$. The position of the center of the circle is always located on the axis of symmetry (Figure 2).

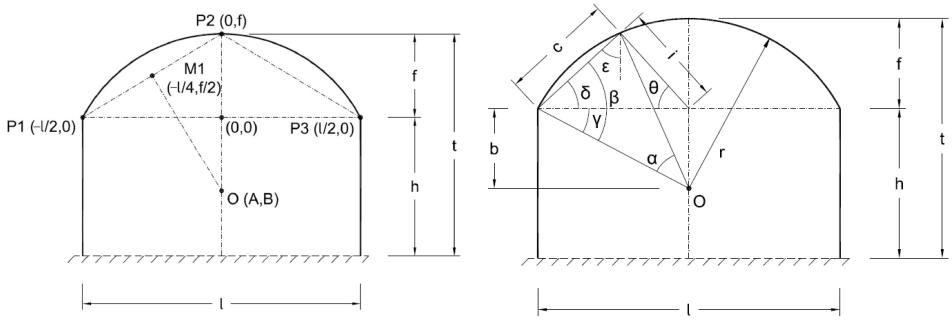

Figure 2. Geometry of a semicylindrical greenhouse span.

The coordinate system is located at the intersection of the axis of symmetry and the line connecting points P1 and P3. The center of the arch, O (A, B), will be contained on the axis of symmetry, where A = 0 (Figure 2). To obtain the coordinate B, we can calculate the equation of the line perpendicular to the line passing through points P1 (−l/2, 0) and P2 (0, f) and passing through the midpoint M1 (−l/4, f/2). The coordinates of the center of the arch are obtained as $O\ (A, B) = (0,\ \frac{f}{2} - \frac{l^2}{8 \cdot f})$, and the radius of the arch is given by r = b + f (Figure 2).

The program allows the length of the arc chord defined by an angle θ and the angle at each point of the cover from the angle δ at each point of the arc to be obtained (Figure 2).

Starting from the isosceles triangle with sides r and c and angle α, we obtain the value of the angle $\beta = (180 - \alpha)/2$ and the angle $\gamma = \arccos(l/2r)$ that define $\delta = \beta - \gamma$. From the triangle formed by sides c, i, and $l/2$, we define $\varepsilon = 90 - \delta$, obtaining $c = 2r(\alpha/2)$, $c_y = c \sin \delta$, and $c_x = c \sin \varepsilon$. With side i being Equation (1), i_x is Equation (2), and the angle θ defining the cover is Equation (3).

$$i = \left(c^2 + \frac{l^2}{4} - c \cdot l \; cos \; cos \; \delta \right)^{\frac{1}{2}} \tag{1}$$

$$i_x = \frac{l}{2} - c_x \tag{2}$$

$$\theta = arc \; cos \; cos \left(\frac{i_x}{i} \right) \tag{3}$$

2.3. Geometric Analysis of Pointed Arches

The pointed arch, also known as "ojival", is composed of two symmetrical circular arches, whose centers are separated by the same distance but in opposite directions with respect to the axis (Figure 3). Depending on the position of the centers, the shape of the arch can vary from a semicylindrical form to a pointed or ogee form. The center of the arch O (A, B) will be contained in the median line that passes through the point M1 (l/4, Y1 + f).

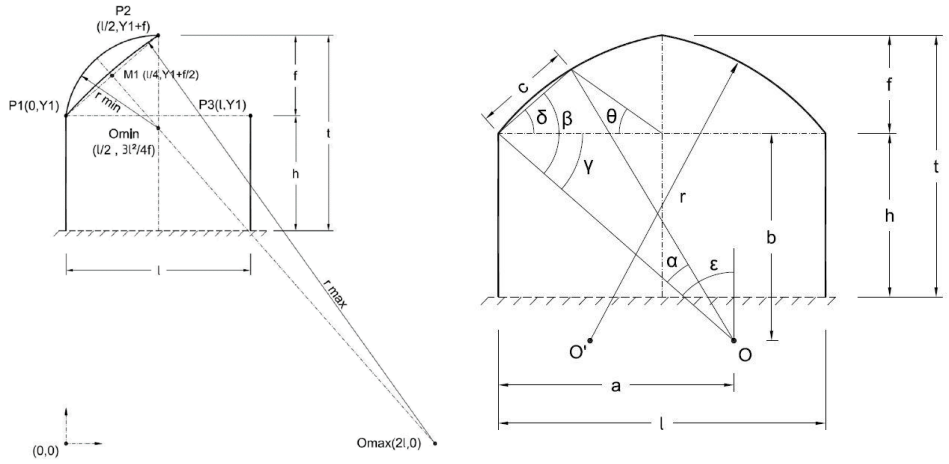

(**a**) (**b**)

Figure 3. Geometry and geometric coordinates of an ogee arch (**a**), Geometric parameters (**b**).

Any pointed arch will be located between the semicylindrical arch form and the triangular gable form, obtained by varying the radius, r, of the arch from a minimum value, r_{min}, with the center at O_{min} (l/2, B_{min}) to a maximum radius, r_{max}, with the center at O_{max} (2l, 0). The values of B_{min} and r_{min} are given in Equations (5) and (6), respectively. Points P1 and P2 are common to all possible arches; we can determine the coordinate Y of point P1 from the equation of the circle with the minimum radius and obtain the maximum radius as r_{max}, as shown in Equation (6).

$$B_{min} = -\frac{l}{2 \cdot f} \cdot \frac{l}{2} + \frac{l^2}{f} = \frac{3 \cdot l^2}{4 \cdot f} \tag{4}$$

$$r_{min} = \frac{f}{2} + \frac{l^2}{8 \cdot f} \leftrightarrow r \; (semicylindrical \; arch) \tag{5}$$

$$r_{max} = \sqrt{(2 \cdot l)^2 + Y1^2} \tag{6}$$

From the dimensions of the arch, f and l, and the obtained coordinates of the center $O(A, B)$ and the radius r, we can establish the relationships between the different angles

that define the cover (Equation (7)), in order to obtain the coordinates of each point on it (Equation (8)) as well as the angle θ (Equation (9)) that the cover traverses (Figure 3b):

$$\varepsilon = arctan\ arctan\left(\frac{a}{b}\right);\ \gamma = 90^\circ - \varepsilon\ ;\ \beta = \frac{180^\circ - \alpha}{2}\ ;\ \delta = \beta - \gamma \tag{7}$$

$$c = 2r\ sin\ sin\left(\frac{\pi}{360^\circ}\alpha\right);\ c_y = c\ sin\ sin\ \delta;\ c_x = c\ cos\delta \tag{8}$$

$$\theta = arc\ tan\ \tan\left(\frac{c_y}{\frac{l}{2} - c_x}\right) \tag{9}$$

It is essential to obtain the angle θ for any greenhouse geometry because, for the strength calculation of the greenhouse [45], the wind action is obtained based on it [46].

2.4. Selection of the Roof Angle

All the previous calculations were implemented in a Matlab program, which allowed us to generate greenhouse models with three roof geometries: semicylindrical, ogee, and gabled. In the design, the roof angle is set to $\mu \geq 30^\circ$ and should be measured at each point along its length according to recommendations from other authors [21]. This value enables snow sliding [17], ensuring structural resistance and optimization in both solar energy capture and solar radiation input. Additionally, with a value of $\mu > 28^\circ$ [36], it minimizes the dripping of condensed water inside the greenhouse. We chose not to increase the roof angle because varying from 28° to 30° reduces light input to the greenhouse by 11.7% [22], and further reductions are not acceptable. However, in arid areas and low latitudes, such as Qatar, a roof inclination of 1:2 is recommended, equivalent to the aspect ratio (width span/length span), when the roof shape is gabled or asymmetrical [16], which is achieved in part by some studied roofs.

3. Results and Discussion

3.1. Analysis and Evaluation of the Roof to Reduce Dripping Due to Condensation

We defined the geometric parameters of the roof shapes considered in this study, which is necessary for calculating the ground surface where condensation water drips from the greenhouse roof.

The program calculates the angle at each point of the curve, μ, for both the semicircular and the gothic or ogee geometries (Figure 4). To do this, it is necessary to know the vertical distance from the center of the arch to the starting point, b, and the span width, l. The position of each point along the length of the arch is defined by its angle (ω + α), where ω is the arc formed by the vertical distance from the center of the arch to the starting point, b, and half of the span width (l/2), and α is the angle from the starting point of the arch to any point on the roof.

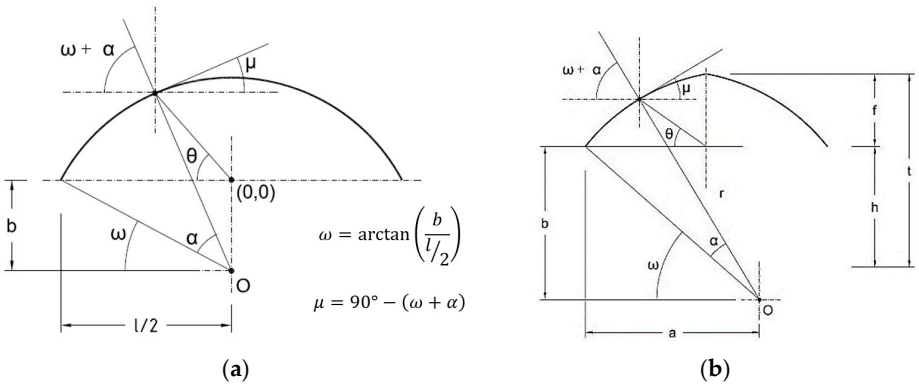

Figure 4. Parameters and relationships for the calculation of the slope of a semicircular roof (**a**), Ojival (**b**).

For angles, μ, greater than or equal to 30°, it is considered that there is no dripping inside the greenhouse, and moreover, it facilitates water collection at the ends of the roof [37,38]. This roof slope value is suitable for various covering materials, including polymethyl methacrylate, commercially known as plexiglass [37], and polyethylene [32,38,39]. Taking advantage of the symmetry of the roof, we calculated the roof inclination angle, μ, only for half of the arch as a function of the angle θ that covers the roof and for different span widths (Figure 5a). Additionally, we also determined the length of the roof with angles less than 30°, which we called "length of roof with precipitation risk", l_{cr}, as well as its horizontal projection, which we called "drip length", l_{cs}. If dripping occurs, it always happens in the central part of the greenhouse (Figure 5b). The greatest length of dripping on the ground, l_{cs}, occurs in semicircular greenhouses.

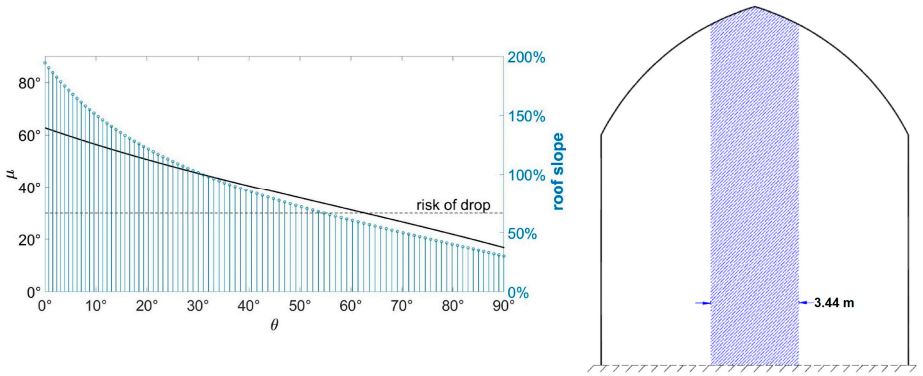

(**a**) (**b**)

Figure 5. (**a**) Roof inclination angle (μ), (**b**) drip length. Greenhouse with l = 12 m, f = 5 m, and h = 9 m.

Next, we studied the geometric evolution of the roof when varying the position of the arches that define it, seeking the one that minimizes the area of the ground on which condensation water can drip. To compare various geometries and make generalizations for any greenhouse, we kept the following parameters constant and equal: the number of bays (n), pillar height (h), and bay length (p).

3.2. Analysis of the Semicylindrical Arch Roof

Next, we aimed to find the semicylindrical form of roof that would result in the least condensation drip inside the greenhouse. In the initial analysis, we studied four types in which we varied the y-coordinate of the arch center at 1/3 of the pillar height, h. Type 1, with center O_1(l/2, 0), corresponds to a semicylindrical roof with a radius of l/2, and type 4, with center at O_4(l/2, −h), represents a nearly flat roof (Figure 6a).

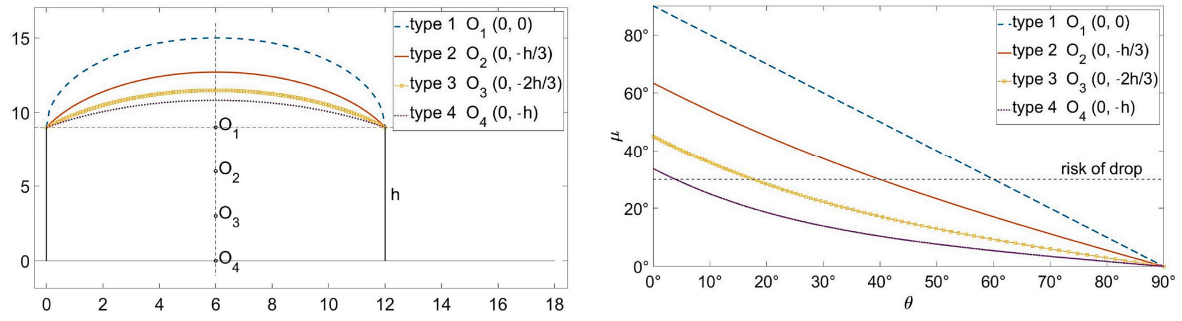

(**a**) (**b**)

Figure 6. Representation of different semicylindrical roofs based on the coordinates of the arch center (**a**). Roof inclination angle, μ, as a function of the angle θ for half of the roof and the different types of semicylindrical arches (**b**).

Given the symmetry of the roof, we considered the calculation of the roof's inclination angle at each point, μ, only for half of it, θ, i.e., between 0° and 90°. The condensed water droplet on the roof will fall into the greenhouse when the roof angle, μ, is less than 30°. For all four types, we observed that μ decreased as it approached the ridge (Figure 6b), facilitating dripping in the central zone of the nave.

Of the four types, the semicylindrical form with the center at O_1 had the longest roof length with angles $\mu \geq 30°$; therefore, the condensation drip will affect the smallest cultivated floor area. As the arch center decreases, so does the ridge height, and the roof length with $\mu < 30°$ increases, affecting a larger cultivation area.

In the greenhouse with a semicylindrical roof, we analyzed the influence of the nave width, l, and the arch height, f, on the condensation water dripping inside the greenhouse. To do this, we calculated the lengths of the roof with a high risk of precipitation, l_{cr}, i.e., with $\mu < 30°$, and the length of the ground that defines the horizontal projection of the said roof, l_{cs}. Additionally, we calculated the percentage of roof area from which dripping occurs, Acr, relative to the total roof area, A_c. We also obtained the percentage of ground area at risk of dripping, A_{cs}, relative to the total ground area under the greenhouse, A_g. The greenhouse length was considered the same for all cases studied.

We analyzed 17 greenhouses with semicylindrical roofs, in which we varied the ridge height from 2 to 6 m, keeping the nave width, l, constant (Figure 7a). We observed that the roof length, l_{cr}, decreased as the arch height, f, decreased but to a lesser extent than the ground width on which dripping would occur, l_{cs}. The variation of A_{cr}/A_c and A_{cs}/A_g was identical, fitting a second-degree polynomial function with $R^2 = 0.9916$. The ground area at risk of dripping, A_{cs}, decreased by 25% when the ridge height increased from 2 to 3 m, 12% when it increased from 3 to 4 m, and only 6.7% and 4.4% when the arch height increased to 5 and 6 m, respectively (Figure 7a). No ridge height was found for which the semicylindrical geometry posed no risk of interior dripping, i.e., $A_{cs} = 0$.

For the study of the influence of porch width, l, we used 19 greenhouse models, in which l varied between 6 and 15 m. The ridge height was kept constant at f = 3 m, a value that favors structural stability without excessively raising construction costs. The results showed that all simulated arches had a high risk of dripping inside the greenhouse (Figure 7). The relationships between A_{cr}/A_c and A_{cs}/A_g fit linear functions, with an $R^2 = 1$ for the latter. In all cases, condensation dripping occurred, and only in widths between 6 and 7.5 m was the affected ground surface, A_{cs}, less than 30% of the total cultivated ground surface, A_g.

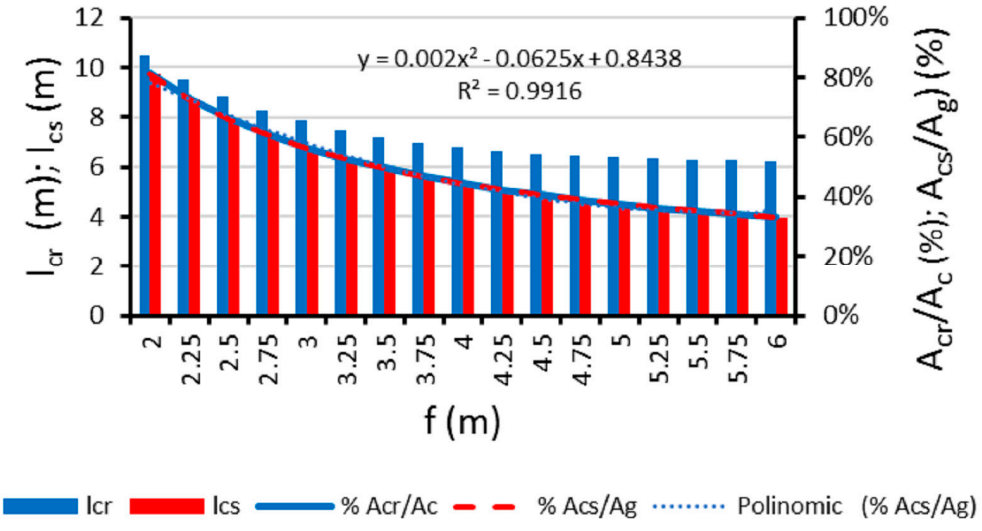

(**a**)

Figure 7. *Cont.*

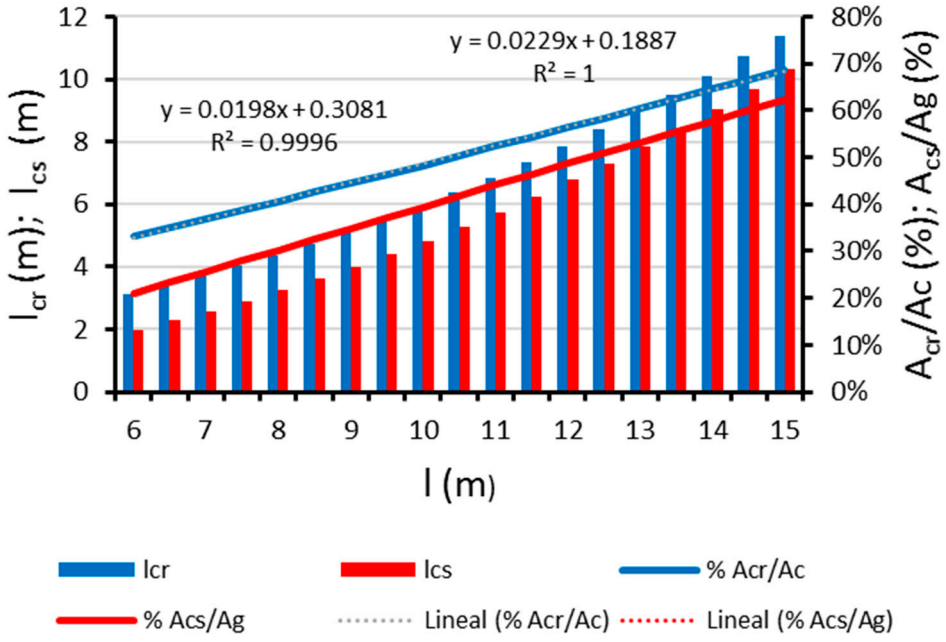

(**b**)

Figure 7. Semicylindrical roof: variation of the length at risk of dripping, l_{cr}, and l_{cs}, when increasing the span width, l (**a**), and arch height, f (**b**).

3.3. Analysis of the Ojival Arch Cover

In the greenhouse with a pointed arch shape (ojival), the roof angle, μ, at each point along its length increased as the radius of the arches defining it increased. Unlike the semicylindrical greenhouse, in the pointed arch, it was possible to find an arch with $\mu \geq 30°$ throughout its length, allowing condensation droplets to slide to the ends and not drip inside the greenhouse. Using a pointed arch with l = 12 m and f = 5 m, we analyzed different center positions, *O*(A,0), defined according to Section 2.2, in order to identify those where the risk of condensation dripping is negligible. We analyzed seven types of pointed arches, varying their center coordinate A by l/4 from a minimum to a maximum value. When A = l/2, we obtained the center of the minimum pointed arch, O_{min} (l/2,0), which corresponded to a semicylindrical roof shape. For A = 2l, we obtained the maximum value, O_{max} (2l,0), and the arch shape had little curvature, resembling a flat, two-pitched roof.

The results showed that the arches with zero risk of dripping, both in roof length, l_{cr}, and its horizontal projection on the ground, lcs, corresponded to those with a coordinate A between 3l/2 and 2l (Figure 8). Additionally, the area of the roof that would produce dripping, A_{cr}, was 38% of the roof area, A_c, in the semicylindrical form (l/2), 18% when A = l, and zero for A = 3l/2 to A = 2l. From this preliminary study, to obtain more significant differences between the types, we chose four of these roof shapes, denoting them with the value of their coordinate A: semicylindrical (type l/2), two-pointed or Gothic (type l and type 3l/2), and two-pitched (type 2l).

Using the Matlab program developed, we calculated the A_{cs}/A_g ratio for the four aforementioned types, where A_{cs} is the area of the soil where dripping would occur, obtained as the horizontal projection of A_{cr}, and A_g is the area of the soil under the greenhouse. For each type, we studied four span widths and four arch heights, f, making up a total of 68 cover geometries. The span widths, l, used were 9, 11, 13, and 15 m, and the maximum arch height, f, ranged from 2.5 to 4 m. The results for the f/l ratios are shown in Table 1, distinguishing between different types of arches [47], denoted as β.

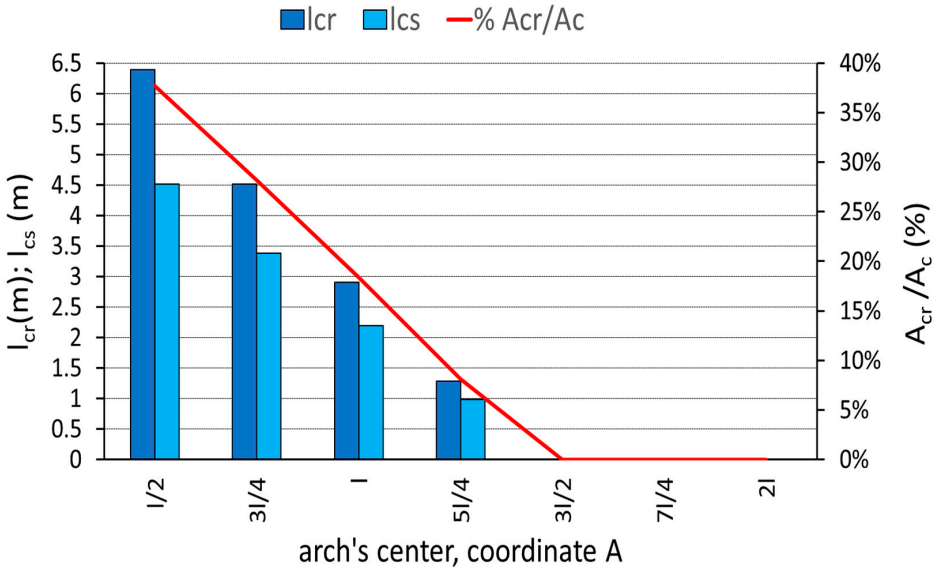

Figure 8. Behavior regarding the dripping of condensed water on the cover for different ogival shapes.

Table 1. Values of span width, *l*; arch height, *f*; and parameter *β*.

***l* (m)**		***f* (m)**			***β* = *f*/*l***			
9	2.5	3	3.5	4	0.278	0.333	0.389	0.444
11	2.5	3	3.5	4	0.228	0.273	0.318	0.363
13	2.5	3	3.5	4	0.192	0.231	0.269	0.308
15	2.5	3	3.5	4	0.167	0.2	0.233	0.267

In the four studied cover shapes, the dripping of condensation inside the greenhouse affected more than 50% of the soil area, A_g, when $\beta \leq 0.278$. The gabled form, type 2l, affected the largest area, while the cylindrical form, type l/2, affected the least area (Figure 9). For higher values, $\beta > 0.278$, the behavior regarding dripping of different greenhouse shapes reversed, and the affected soil area was less than 50%, with the gabled cover affecting the least area and the cylindrical cover affecting the most. In the semicircular greenhouse, dripping affected more than 35% of the soil area, A_g, in all cases studied, while it became zero for the ogival forms, 3l/2, and gabled, 2l, when $\beta > 0.389$ and >0.363, respectively. We concluded that dripping does not occur on the crop only in those arcs with smaller widths (l = 9 m) and greater heights (f = 4 and 3.5 m).

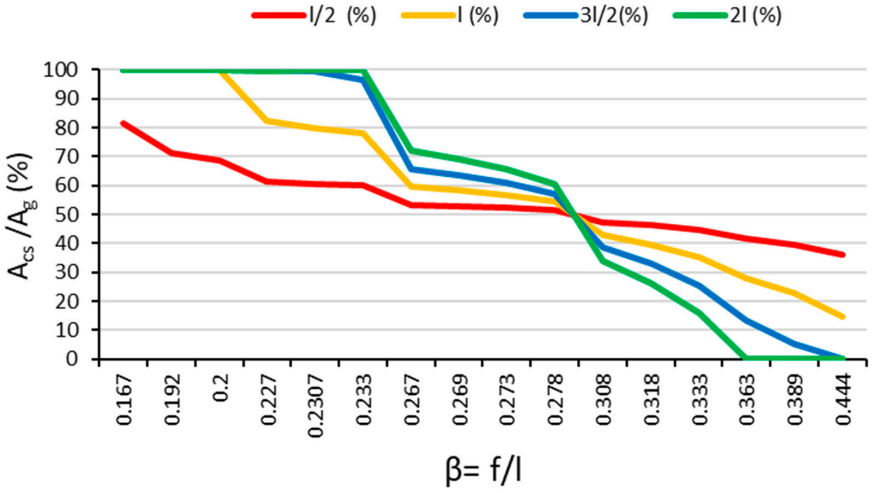

Figure 9. A_{cs}/Ag across the four types of cover studied when varying the parameters *f* and *l*.

3.4. Influence of the Cover Shape on the Greenhouse Volume

The height of the greenhouse determines the unit volume of air inside and its thermal inertia [1]. Taller greenhouses have greater thermal inertia and improve ventilation efficiency. Under equal design parameters, those with a semicircular cover, $l/2$, enclose the greatest volume of air, while those with a straight gable cover enclose the least. In this study, we considered the four cover shapes from the previous section, namely, types $l/2$, l, $3l/2$, and $2l$, to determine which cover shape would be most suitable under different climatic conditions.

We defined the following design parameters: number of spans (n), span width (l), pillar height, h; span length, p; arc length, l_c; the angle that defines the cover, μ; and the transversal cover area, A_{ct}. To calculate the volume of air inside the greenhouse (Equation (10)) and make it dependent only on the cover shape, we kept the parameters n and p constant. The pillar height, h, was set at 6 m.

$$V = n \cdot p \cdot \left(l \cdot h + \int_0^{\mu} l_c \cdot d\mu \right) = n \cdot p \cdot (l \cdot h + A_{ct}) \tag{10}$$

The volume of air depends on the number of spans and the length of the greenhouse, allowing a comparison of different greenhouse shapes when a specific value for h is fixed. For h = 6 m, it was observed that the total area was larger in the semicircular greenhouse, $l/2$, and smaller in the gable roof, $2l$ (Figure 10a). When comparing the transversal cover area, A_{ct} (Figure 10b), with the total area (Figure 10a), it was found that the volume primarily depended on the pillar height [48]. The volume did not correlate with the growth of β.

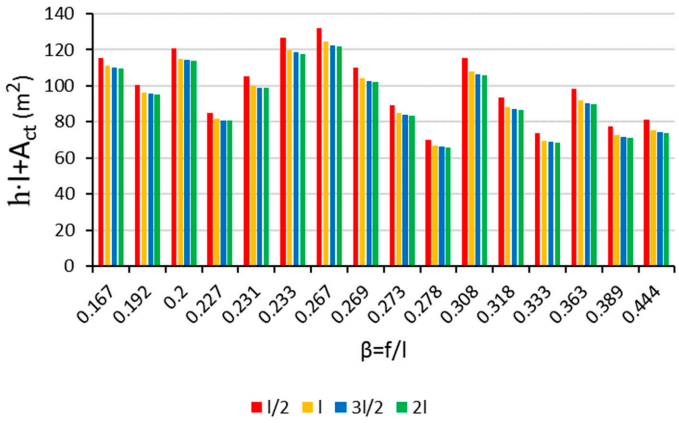

(**a**)

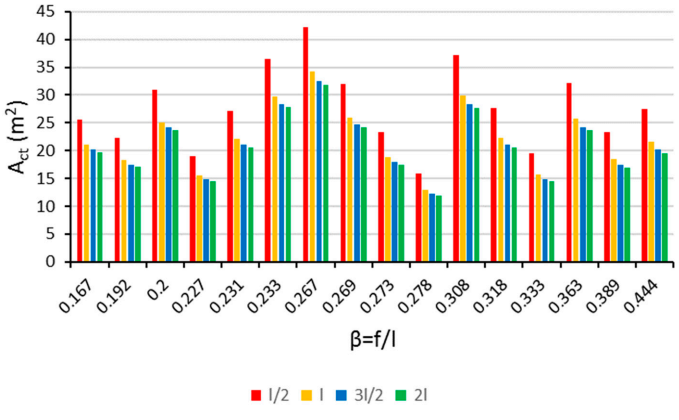

(**b**)

Figure 10. Increase in the greenhouse interior air volume: (**a**) varying the span width, (**b**) varying the pitch height.

A greater greenhouse volume can lead to a reduction in energy consumption per kilogram of product produced [25]. Various authors have employed greenhouse volume to compare different types of structures [24] or to conduct the corresponding energy balance [1,13]. Greenhouse volume determines the ventilation ratio or mass flow rate [5].

Greenhouse types that minimize condensation dripping inside correspond to those with smaller l and larger f, i.e., with $\beta \geq 0.363$, and the volume of air due to the shape of the cover is similar compared to those with $\beta \leq 0.2$. Therefore, it is possible to find relationships between the cover angle and span width that optimize both condensation sliding and the volume of air inside the greenhouse. Thus, for all cover heights tested, a span width of 9 m met both conditions, and for a span width of 11 m, cover heights of 3.5 and 4 m also met the criteria.

Finally, there was only a maximum difference of 1% in the volume of interior air between the $3l/2$ and $2l$ shapes, so this would not be a deciding factor between them.

3.5. Influence of the Roof Type on Heat Losses and Gains

The energy efficiency of a greenhouse is closely tied to the amount of fossil energy needed for heating or cooling its interior. In this context, the roof's shape plays a crucial role in influencing both the receipt of solar radiation and the heat losses to the exterior. Although the four types of greenhouses studied exhibit negligible variations in roof angle along their length, significant differences in roof surface impact the overall energy efficiency of each greenhouse.

To quantify this, we calculated the roof surface, which depends only on the arc length, l_{ar}, assuming a constant greenhouse length, p, for all greenhouse types studied. Our findings indicated that semicircular roof greenhouses had a longer arc length than ojival roofs, with very small differences among the ojival types when compared for the same width, l, and height, f. The semicircular roof had 10% more surface area than the other forms, while the difference between the ojival forms was 0.2%. These percentages decreased with increasing span width.

Therefore, in terms of solar energy capture by the roof surface, semicircular greenhouses would be more efficient [49], with almost two-walled ojival ones being the least efficient. However, it was observed that similar arc length values could be obtained for different width values (Figure 11). Therefore, the efficiency of the roof cannot be determined using the ratio $= f/l$ as it does not show growth or decline when A_c does.

To provide a more comprehensive comparison of different greenhouse roof forms when f and l vary, it is recommended to calculate both solar radiation capture and heat losses using the ratio A_c/A_g, defined as the ratio of the roof surface A_c to the cultivated ground surface A_g [15,49]. The results for the four roof types (Figure 11b) show that as the value of β increases, the Ac/Ag ratio also increases. Depending on the season, the efficiency of capturing solar energy varies.

During winter, increasing the height of the roof, f, and decreasing the span width, l, increases solar energy capture [50]. The semicircular roof, $l/2$, remains the one that will capture the most solar energy for any β value, followed, in decreasing order, by types l, $3l/2$, and $2l$, with the most efficient corresponding to the roof with the smallest width (l = 9 m) and roof height (f = 4 and 3.5 m).

However, from June to September, the curved surface with an ojival shape will absorb less solar radiation as the height, f, increases in relation to the width, l. In contrast, from December to March, the opposite occurs when compared to an inclined flat surface [15]. Therefore, ojival-shaped roofs become less efficient at capturing solar energy as β increases and the roof surface becomes larger. For this reason, these roofs are more suitable for greenhouses in warm climates at middle latitudes.

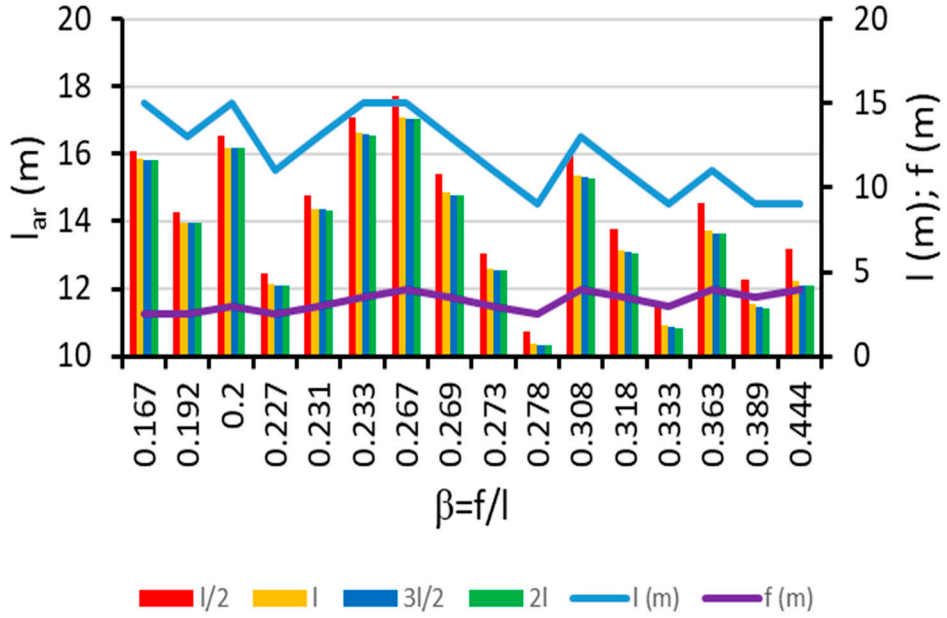

(**a**)

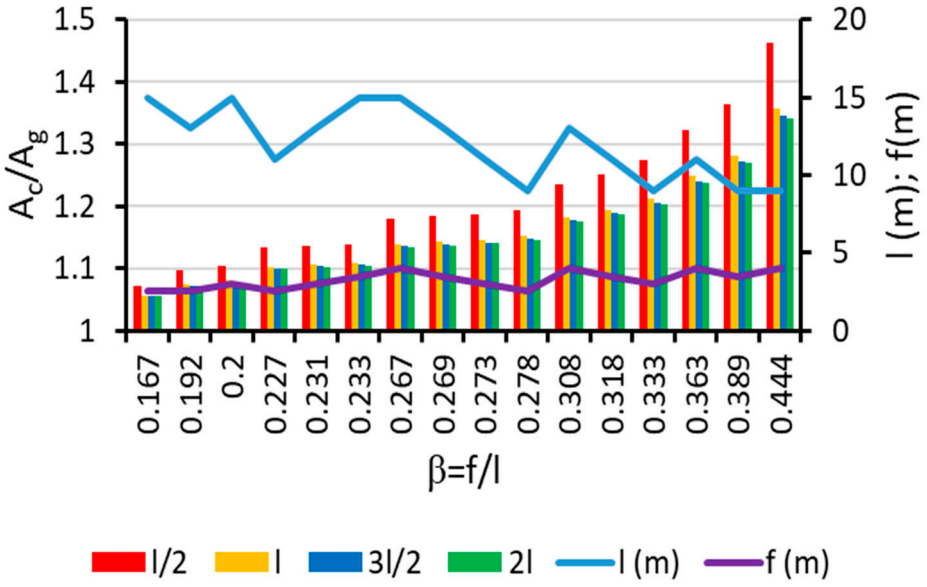

(**b**)

Figure 11. Relationships between the roof and its geometry (surface of β). (**a**) l_{ar}. (**b**) A_c/A_g.

On the other hand, it should be considered that the higher the ratio between the roof surface and the ground surface, A_c/A_g, the greater the thermal exchange with the external environment. This results in higher energy consumption for heating or cooling the interior [49]. Thus, in cold and very warm climates, the least energy-efficient roofs would be those with high values of A_c/A_g and β as a larger roof surface causes greater heat losses [17]. Additionally, in desert climates, the increased water consumption of evaporative cooling systems is particularly relevant [51].

In summary, greenhouses with arched roofs exhibit varying energy efficiency throughout the year, with semicircular roofs favored in cold climates and ojival roofs in warm climates. Greenhouses with arched roofs require less energy for heating during winter, and the opposite occurs during summer [12]. In warm climates, the semicircular arched shape, with its low f/l, would require less energy annually. However, several authors have

studied the energy needs of various greenhouse shapes, finding that the most efficient shape is similar to the gothic form, type *l*, studied in this work [12,52].

In warm climates and low to mid-latitudes, when cooling needs exceed heating and natural ventilation is the primary cooling method, roofs with a higher A_c/A_g ratio and a greater angle at all points are the ones that require less energy annually. Therefore, the recommendation is for the ogee-shaped (type l) roof with narrower spans (l = 9 m).

In cold climates and high latitudes, high roof angles are recommended to increase solar energy capture, along with low values for the A_c/A_g ratio to minimize heat losses. The ogee-shaped roof, specifically type $3l/2$ with small β values (larger spans), is advisable, as suggested by other authors [17].

Finally, the most energy-efficient greenhouse is the one with the smallest exterior surface area relative to the covered floor area. The energy consumption for heating can increase by up to 42% in single-span greenhouses compared to multitunnel structures [25]. Therefore, in extreme climates, roofs with a lower A_c/A_g ratio and β values are recommended, especially for multispan greenhouses.

3.6. Impact of Greenhouse Length on Energy Efficiency

We calculated the ratio of the total area of the greenhouse cover, including the cover and end walls (A_{ct}), to the ground area (A_g), i.e., A_{ct}/A_g, for the studied greenhouse models ($l/2$, l, $3l/2$, and $2l$) using four greenhouse lengths (25, 50, 100, and 150 m). The results showed that beyond 100 m, the A_{ct}/A_g ratio barely varied (Figure 12).

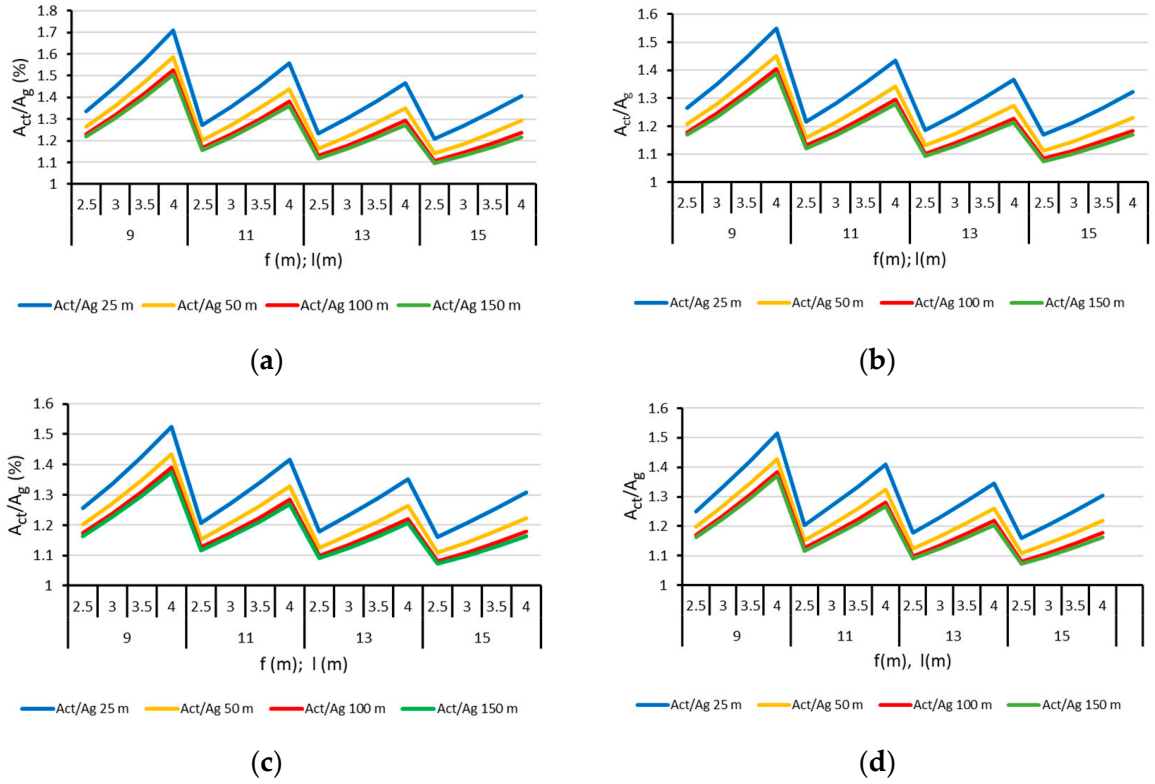

Figure 12. Variation of A_{ct}/A_g for greenhouse lengths of 25, 50, 100, and 150 m for the different studied greenhouse types: (**a**) $l/2$, (**b**) l, (**c**) $3l/2$, and (**d**) $2l$.

It was observed that in the semicircular greenhouse model, $l/2$, the highest values of cover area in relation to cultivated soil were obtained. This type of cover would capture the most solar radiation but also have the highest heat exchange with the exterior [14]. In general, in all models, the greatest decrease in the ratio corresponded to a length of 50 m. A larger cover area increases heat losses through it, which is particularly relevant in multispan greenhouses [25] as the cover surface is significantly larger than the sidewalls.

The length of the greenhouse would not influence energy losses through the cover surface by conduction beyond 100 m. The optimal size of the greenhouse in arid climates will have a ratio between its width and length of 0.5 [16], thus being 50 m wide and 100 m long.

4. Conclusions

The developed program allows the calculation of various geometric parameters for both semicylindrical and ovoidal arches. By varying both the span width, l, and the arch height, f, any geometry ranging from an arch with a radius of $l/2$ to a flat or triangular surface can be obtained.

Ovoidal (ojival) cover shapes facilitate the sliding of condensed water droplets on the greenhouse cover, preventing interior dripping. It is not possible to find a semicylindrical shape that does not result in condensation water dripping into the greenhouse interior.

The volume of air inside the greenhouse depends primarily on the pillar height, with small differences attributable to the shape of the cover.

Solar radiation capture by the greenhouse cover increases for high values of A_c/A_g and β, which is achieved with narrower spans and higher arch heights (3–4 m). Accordingly, we classified the studied cover types in decreasing order of solar energy capture efficiency: $l/2$, l, $3l/2$, and $2l$. However, only types $3l/2$ and $2l$ would not result in interior dripping within the greenhouse.

As the cover angle increases, the A_c/A_g ratio also increases, leading to higher heating demands during winter. If the angle is too low, snow accumulation could pose a risk to the structure in northern latitudes, meaning an angle of 25–30° is recommended to allow for snow sliding.

In warm climates and medium to low latitudes, where cooling needs outweigh heating and natural ventilation is the primary cooling method, covers with a higher A_c/A_g ratio and a greater angle at all points require less energy annually. Additionally, these are the types that do not result in interior dripping within the greenhouse. Therefore, the ovoidal shape $3l/2$ and smaller span widths, such as 9 m, are recommended.

Ovoidal cover shapes have a lower A_c/A_g ratio than the semicircular form, reducing energy losses, especially for low β values. In cold climates and high latitudes, the ovoidal shape, l, is recommended due to its higher angles throughout its length compared to the two-way shape, $2l$, and only a small difference in total surface area between them. This increases solar energy capture and decreases heat losses through the cover. Larger span widths of 13 and 15 m with a 2.5 m arch height are preferable. However, with these dimensions, the roof slope angle does not allow for the sliding of condensation droplets, resulting in interior dripping within the greenhouse.

Author Contributions: Conceptualization, A.P.-F. and P.M.; methodology, A.P.-F.; software, M.A.C.-R.; validation, A.P.-F., P.M. and M.A.C.-R.; formal analysis and investigation, A.P.-F. and P.M.; resources and data curation, M.A.C.-R.; writing—original draft preparation and writing—review and editing, A.P.-F.; visualization, P.M.; supervision, project administration, and funding acquisition, A.P-F. All authors have read and agreed to the published version of the manuscript.

Funding: The FEDER-Andalucía 2014–2020 operation program. via the research project UAL2020-TEP-A1986, funded this research.

Institutional Review Board Statement: Not applicable.

Data Availability Statement: The data that support this study are available from the corresponding author upon reasonable request.

Acknowledgments: The authors wish to express their gratitude to the research center CIAIMBITAL of the University of Almería (Spain) for their support throughout the development of this study.

Conflicts of Interest: The authors declare no conflicts of interest. The funders had no role in the design of the study; in the collection, analyses, or interpretation of data; in the writing of the manuscript; or in the decision to publish the results.

References

1. Valera, D.L.; Belmonte, L.J.; Molina, F.D.; López, A. *Greenhouse Agriculture in Almeria. A Comprehesive Tecno-Economic Analysis*; Cajamar Caja Rural: Almería, Spain, 2016; 408p. Available online: http://www.publicacionescajamar.es/series-tematicas/economia/greenhouse-agriculture-in-almeria-a-comprehensive-techno-economic-analysis/ (accessed on 26 December 2023).
2. Mendoza-Fernández, A.J.; Peña-Fernández, A.; Molina, L.; Aguilera, P.A. The role of technology in greenhouse agriculture: Towards a sustainable intensification in campo de Dalías (Almería, Spain). *Agronomy* **2021**, *11*, 101. [CrossRef]
3. Baneshi, M.; Gonome, H.; Maruyama, S. Wide-range spectral measurement of radiative properties of commercial greenhouse covering plastics and their impacts into the energy management in a greenhouse. *Energy* **2020**, *210*, 118535. [CrossRef]
4. Gupta, M.J.; Chandra, P. Effect of greenhouse design parameters on conservation of energy for greenhouse environmental control. *Energy* **2002**, *27*, 777–794. [CrossRef]
5. Kumari, N.; Tiwari, G.N.; Sodha, M.S. Performance Evaluation of Greenhouse having Passive or Active Heating in Different Climatic Zones of India. *Agric. Eng. Int. CIGR E-J.* **2007**, *9*, 1–19.
6. Sethi, V.P. On the selection of shape and orientation of a greenhouse: Thermal modeling and experimental validation. *Sol. Energy* **2009**, *83*, 21–38. [CrossRef]
7. Ahamed, M.S.; Guo, H.; Tanino, K. A quasi-steady state model for predicting the heating requirements of conventional greenhouses in cold regions. *Inf. Process. Agric.* **2018**, *5*, 33–46. [CrossRef]
8. Ahamed, M.S.; Guo, H.; Tanino, K. Energy saving techniques for reducing the heating cost of conventional greenhouses. *Biosyst. Eng.* **2019**, *178*, 9–33. [CrossRef]
9. Stanciu, C.; Stanciu, D.; Dobrovicescu, A. Effect of Greenhouse Orientation with Respect to E-W Axis on its Required Heating and Cooling Loads. *Energy Procedia* **2016**, *85*, 498–504. [CrossRef]
10. Xu, D.; Li, Y.; Zhang, Y.; Xu, H.; Li, T.; Liu, X. Effects of orientation and structure on solar radiation interception in Chinese solar greenhouse. *PLoS ONE* **2020**, *15*, e0242002. [CrossRef]
11. Mobtaker, H.G.; Ajabshirchi, Y.; Ranjbar, S.F.; Matloobi, M. Solar energy conservation in greenhouse: Thermal analysis and experimental validation. *Renew. Energy* **2016**, *96*, 509–519. [CrossRef]
12. Choab, N.; Allouhi, A.; Maakoul, A.E.; Kousksou, T.; Saadeddine, S.; Jamil, A. Effect of Greenhouse Design Parameters on the Heating and Cooling Requirement of Greenhouses in Moroccan Climatic Conditions. *IEEE Access* **2021**, *9*, 2986–3003. [CrossRef]
13. Singh, R.D.; Tiwari, G.N. Energy conservation in the greenhouse system: A steady state analysis. *Energy* **2010**, *35*, 2367–2373. [CrossRef]
14. Çakir, U.; Şahin, E. Using solar greenhouses in cold climates and evaluating optimum type according to sizing, position and location: A case study. *Comput. Electron. Agric.* **2015**, *117*, 245–257. [CrossRef]
15. Tanaka, H.; El-Maghlany, W.M.; Teamah, M.A. Analytical study on solar energy absorbed on elliptic curved collector. *Sol. Energy* **2015**, *115*, 667–679. [CrossRef]
16. Ghani, S.; El-Bialy, E.M.; Bakochristou, F.; Rashwan, M.M.; Abdelhalim, A.M.; Ismael, S.M.; Ben, P. Experimental and numerical investigation of the thermal performance of evaporative cooled greenhouses in hot and arid climates. *Sci. Technol. Built Environ.* **2020**, *26*, 141–160. [CrossRef]
17. Ahamed, M.S.; Guo, H.; Tanino, K. Energy-efficient design of greenhouse for Canadian Prairies using a heating simulation model. *Int. J. Energy Res.* **2018**, *42*, 2263–2272. [CrossRef]
18. Sharshir, S.W.; Eltawil, M.A.; Algazzar, A.M.; Sathyamurthy, R.; Kandeal, A.W. Performance enhancement of stepped double slope solar still by using nanoparticles and linen wicks: Energy, exergy and economic analysis. *Appl. Therm. Eng.* **2019**, *174*, 115278. [CrossRef]
19. Soriano, T.; Montero, J.I.; Sánchez-Guerrero, M.C.; Medrano, E.; Antón, A.; Hernández, J.; Morales, M.I.; Castilla, N. A Study of direct solar radiation transmission in asymmetrical multi-span greenhouses using scale models and simulation models. *Biosyst. Eng.* **2004**, *88*, 243–253. [CrossRef]
20. Esmaeli, H.; Roshandel, R. Optimal design for solar greenhouses based on climate conditions. *Renew. Energy* **2020**, *145*, 1255–1265. [CrossRef]
21. Huang, L.; Deng, L.; Li, A.; Gao, R.; Zhang, L.; Lei, W. Analytical model for solar radiation transmitting the curved transparent surface of solar greenhouse. *J. Build. Eng.* **2020**, *32*, 101785. [CrossRef]
22. Yang, W. Simulation study on the influence of roof inclination on the light environment of solar greenhouse. *IOP Conf. Ser. Earth Environ. Sci.* **2021**, *621*, 012115. [CrossRef]
23. Rasheed, A.; Kwak, C.S.; Kim, H.T.; Lee, H.W. Building energy an simulation model for analyzing energy saving options of multi-span greenhouses. *Appl. Sci.* **2020**, *10*, 6884. [CrossRef]
24. Jagadeesh, D.; Vivekanandan, M.; Natarajan, A.; Chandrasekar, S. Experimental conditions to identify the ideal shape of dryer investigation of six shapes of solar greenhouse dryer in no load. *Mater. Today Proc.* **2020**, *37*, 395–403. [CrossRef]
25. Djevic, M.; Dimitrijevic, A. Energy consumption for different greenhouse constructions. *Energy* **2009**, *34*, 1325–1331. [CrossRef]
26. Tong, X.; Sun, Z.; Sigrimis, N.; Li, T. Energy sustainability performance of a sliding cover solar greenhouse: Solar energy capture aspects. *Biosyst. Eng.* **2018**, *176*, 88–102. [CrossRef]
27. Cemek, B.; Demir, Y. Testing of the condensation characteristics and light transmissions of different plastic film covering materials. *Polym. Test.* **2005**, *24*, 284–289. [CrossRef]

28. Pollet, I.V.; Pieters, J.G. PAR transmittances of dry and condensate covered glass and plastic greenhouse cladding. *Agric. For. Meteorol.* **2002**, *110*, 285–298. [CrossRef]
29. Pollet, I.V.; Pieters, J.G.; Deltour, J.; Verschoore, R. Diffusion of Radiation Transmitted through Dry and Condensate Covered Transmitting Materials. *Sol. Energy Mater. Sol. Cells* **2005**, *86*, 177–196. [CrossRef]
30. Hoeniges, J.; Zhu, K.; Pruvost, J.; Legrand, J.; Si-Ahmed, E.K.; Pilon, L. Impact of dropwise condensation on the biomass production rate in covered raceway ponds. *Energies* **2021**, *14*, 268. [CrossRef]
31. Durán, I.R.; Laroche, G. Water drop-surface interactions as the basis for the design of anti-fogging surfaces: Theory, practice, and applications trends. *Adv. Colloid Interface Sci.* **2019**, *263*, 68–94. [CrossRef]
32. Santos, M.J.; Velasco, S.; White, J.A. Simulation analysis of contact angles and retention forces of liquid drops on inclined surfaces. *Langmuir* **2012**, *28*, 11819–11826. [CrossRef] [PubMed]
33. Ruiz-Cabello, F.J.M.; Rodríguez-Valverde, M.A.; Cabrerizo-Vílchez, M. A new method for evaluating the most stable contact angle using tilting plate experiments. *Soft Matter* **2011**, *7*, 10457–10461. [CrossRef]
34. White, J.A.; Santos, M.J.; Rodríguez-Valverde, M.A.; Velasco, S. Numerical study of the most stable contact angle of drops on tilted surfaces. *Langmuir* **2015**, *31*, 5326–5332. [CrossRef] [PubMed]
35. Venkateshan, D.G.; Tafreshi, H.V. Modelling droplet sliding angle on hydrophobic wire screens. *Colloids Surf. A Physicochem. Eng. Asp.* **2018**, *538*, 310–319. [CrossRef]
36. Xu, H.; Yuan, Z.; Lee, J.; Matsuura, H.; Tsukihashi, F. Contour evolution and sliding behavior of molten Sn-Ag-Cu on tilting Cu and Al2O3 substrates. *Colloids Surf. A Physicochem. Eng. Asp.* **2010**, *359*, 1–5. [CrossRef]
37. Beysens, D.; Milimouk, I.; Nikolayev, V.; Muselli, M.; Marcillat, J. Using radiative cooling to condense atmospheric vapor: A study to improve water yield. *J. Hydrol.* **2003**, *276*, 1–11. [CrossRef]
38. Maestre-Valero, J.F.; Ragab, R.; Martínez-Alvarez, V.; Baille, A. Estimation of dew yield from radiative condensers by means of an energy balance model. *J. Hydrol.* **2012**, *460–461*, 103–109. [CrossRef]
39. Briscoe, B.J.; Galvin, K.P. The sliding of sessile and pendent droplets The critical condition. *Colloids Surf.* **1991**, *52*, 219–229. [CrossRef]
40. Khandekar, S.; Muralidhar, K. Dropwise Condensation: Simulation Results. In *Dropwise Condensation on Inclined Textured Surfaces. SpringerBriefs in Applied Sciences and Technology*; Springer: New York, NY, USA, 2014. [CrossRef]
41. Sikarwar, B.S.; Khandekar, S.; Muralidhar, K. Mathematical modelling of dropwise condensation on textured surfaces. *Sadhana* **2013**, *38*, 1135–1171. [CrossRef]
42. Thampi, S.P.; Govindarajan, R. Minimum energy shapes of one-side-pinned static drops on inclined surfaces. *Phys. Rev. E* **2011**, *84*, 046304. [CrossRef]
43. Alcayde, A.; Velilla, C.; San-Antonio-Gómez, C.; Peña-Fernández, A.; Pérez-Romero, A.; Manzano-Agugliaro, F. Basket-Handle Arch and Its Optimum Symmetry Generation as a Structural Element and Keeping the Aesthetic Point of View. *Symmetry* **2019**, *11*, 1243. [CrossRef]
44. Urruchi-Rojo, J.R.; Martínez-Martínez, J.A.; Serrano-lópez, R. De la bóveda de medio punto a la bóveda escarzana en los puentes de piedra. Influencia del rebajamiento y del relleno rígido en la variación de la carga de rotura. *Inf. Constr.* **2017**, *69*, 545. [CrossRef]
45. Maraveas, C.; Tsavdaridis, K.D. Strengthening Techniques for Greenhouses. *AgriEngineering* **2020**, *2*, 37–54. [CrossRef]
46. Maraveas, C. Wind Pressure Coefficients on Greenhouse Structures. *Agriculture* **2020**, *10*, 149. [CrossRef]
47. Serrano-López, R.; Urruchi-Rojo, J.R.; Martínez-Martínez, J.A. The shallow arch: A step towards bridges styling in the early 19th century. *Eng. Struct.* **2017**, *167*, 84–95. [CrossRef]
48. Vanthoor, B.H.E.; van Henten, E.J.; Stanghellini, C.; de Visser, p.H.B. A methodology for model-based greenhouse design: Part 3, sensitivity analysis of a combined greenhouse climate-crop yield model. *Biosyst. Eng.* **2011**, *110*, 396–412. [CrossRef]
49. Chen, J.; Ma, Y.; Pang, Z. A mathematical model of global solar radiation to select the optimal shape and orientation of the greenhouses in southern China. *Sol. Energy* **2020**, *205*, 380–389. [CrossRef]
50. El-Maghlany, W.M.; Teamah, M.A.; Tanaka, H. Optimum design and orientation of the greenhouses for maximum capture of solar energy in North Tropical Region. *Energy Convers. Manag.* **2015**, *105*, 1096–1104. [CrossRef]
51. Tsafaras, I.; Campen, J.B.; Stanghellini, C.; de Zwart, H.F.; Voogt, W.; Scheffers, K.; Harbi, A.A.; Assaf, K.A. Intelligent greenhouse design decreases water use for evaporative cooling in arid regions. *Agric. Water Manag.* **2021**, *250*, 106807. [CrossRef]
52. Gracely, B.; Tarver, K.; Josifek, H.; Ahamed, M.S. Effect of Shape and Orientation on the Thermal Performance of Greenhouses in the Western USA. In Proceedings of the 2021 ASABE Annual International Virtual Meeting, Online, 12–16 July 2021; American Society of Agricultural and Biological Engineers: St. Joseph, MI, USA, 2021; p. 1. [CrossRef]